Nuclear Engineering and Technology 56 (2024) 4734–4747

Contents lists available at ScienceDirect

Nuclear Engineering and Technology

journal homepage: www.elsevier.com/locate/net

Original Article

Advanced interpretation of the SPHERE irradiation experiment with neutronics and fuel performance codes

Marc Lainet [a,*], Lelio Luzzi [b], Alessio Magni [b], Davide Pizzocri [b], Martina Di Gennaro [b], Paul Van Uffelen [c], Arndt Schubert [c], Elio D'Agata [c], Vincenzo Romanello [d], Andrei Rineiski [e], Karl Sturm [e], Sander Van Til [f], Florence Charpin [f], Alexander Fedorov [f]

[a] Commissariat à l'Énergie Atomique et aux Énergies Alternatives (CEA), France
[b] Politecnico di Milano (POLIMI), Italy
[c] Joint Research Centre (JRC), Germany
[d] Centrum výzkumu Řež (CVR), Czech Republic
[e] Karlsruher Institut für Technologie (KIT), Germany
[f] Nuclear Research and consultancy Group (NRG), the Netherlands

ARTICLE INFO

Keywords:
SPHERE irradiation experiment
Minor actinide-bearing driver fuel
Neutronics tools
Fuel performance codes
Assessment and benchmark

ABSTRACT

The SPHERE experiment aimed at studying the behaviour of Minor Actinide-bearing Driver Fuel (U,Pu,Am)O_{2-x} by comparing sphere-packed and pelletized fuels. The irradiation experiment was performed in the High Flux Reactor at Petten from August 2013 to April 2015, and was followed by post-irradiation examinations up to mid-2017. The present work consists in a new analysis of the SPHERE experiment, focusing on the pelletized fuel, by the means of both neutronics and fuel performance codes. This study is performed in the frame of the European Project PATRICIA. The adopted methodology and the main results achieved, assessed in particular against inert gas-related experimental data, are presented in the paper.

1. Introduction

The SPHERE experiment [1,2] aimed at studying the behaviour of Minor Actinide-bearing Driver Fuel (MADF) by comparing sphere-packed and pelletized fuels. It consists of two pins with (U,Pu,Am)O_{2-x} fuel (~3 wt% Am) irradiated in the HFR (High Flux Reactor, Petten). The pins were stored for seven months before post-irradiation examinations (PIEs). We focus here on pin #1 that contains 10 fuel pellets in a stack. The SPHERE program (fabrication, irradiation and experimental investigations) was part of the former European Projects FAIRFUELS [3] and PELGRIMM [4]. The post-irradiation examinations were performed during the PELGRIMM Project along with a first assessment of the experiment with fuel performance codes (FPCs). The SPHERE experiment is now re-analysed within the PATRICIA Project [5], which focuses on advancements on partitioning and transmutation of Am-fuels. Hence, SPHERE is considered as an experimental case of reference for the advancement and assessment of FPCs, through a benchmark process. Dedicated neutronics modelling of the SPHERE experiment are also performed, given the peculiar irradiation set-up in the HFR. The chaining of neutronics simulations of the device with FPCs computations thus represents an important methodological progression to simulate the SPHERE irradiation, with the goal to improve the reliability of the predictions for such experiment performed in a material testing reactor.

A brief description of the SPHERE experiment is provided in Section 2. Then, Section 3 focuses on the codes applied in this study, and explains the principle of the chaining between the neutronics simulations and the FPCs. The resulting advanced interpretation of SPHERE is presented in Section 4, dealing first with the neutronics analysis, then with the fuel element behaviour predicted by the fuel performance codes involved in this study. The discussion of the results is focusing first on the fission gas (Xe, Kr) behaviour but also on helium, which represents a major concern for minor actinide-bearing fuels. The predictions obtained for the fuel restructuring mechanism are also presented and discussed. Some perspectives for further evolutions of the simulation tools are proposed in the Conclusion, along with some considerations about the assessment of the modelling involved in the fuel performance codes against such an experiment like SPHERE.

* Corresponding author. CEA (French Alternative Energies and Atomic Energy Commission), France.
E-mail address: marc.lainet@cea.fr (M. Lainet).

https://doi.org/10.1016/j.net.2024.06.037
Received 21 March 2024; Received in revised form 19 June 2024; Accepted 20 June 2024
Available online 22 June 2024

2. The SPHERE experiment in the HFR

The SPHERE irradiation was carried out in the HFR from August 28, 2013 till December 30, 2014 always maintaining a constant irradiation temperature of the fuel, as illustrated on the following Fig. 1 showing the monitoring of the middle-height cladding temperatures of both fuel pins. In Fig. 1, the pin #1 with pelletized fuel is referred as "bottom pin", and the pin #2 with sphere-packed fuel is referred as "top pin", with regards to their respective locations in the sample holder.

A detailed description of the experiment is provided in [1]. The fuel irradiated was a Minor Actinide-bearing Driver Fuel containing about 3 % americium and 20 % Plutonium. The main characteristics and composition of SPHERE fuel are given in the following Table 1.

The fuel irradiated was in the form of:

- pellets of an average diameter of 5.38 mm stacked one on top of the other for a total length of 58 mm, held in place with a spring. Two pellets of Hf have been placed at the top and at the bottom of the fuel stack in order to decrease the power peaking at the edge of the fuel stack. A drawing of the SPHERE pin #1 with pelletized fuel is given by Fig. 2;
- sphere-pac fuel, composed of small spherical pebbles of two sizes, 0.8 and 0.05 mm, to enhance the packing density. Also the sphere-pac fuel stack had two Hf pellets at either end to keep the sphere-pac in place and to minimize power peaking.

The two pins made of 15-15 Ti steel and containing pellets and sphere-pac fuel in an inert environment (helium) were contained into an assembly which comprises two sample holders made of stainless steel one inside the other:

- the internal sample holder was containing the two pins immersed in a bath of sodium and equipped with thermocouples, fluence detectors and pressure transducers;
- the external sample holder, containing the internal sample holder and its content, was surrounded with a liner of Hafnium foils (0.8 mm thick) in order to harden the neutron spectrum. It is thus important to underline here that the device was designed with the goal to create inside the HFR experimental conditions representative of those in a fast spectrum reactor. Finally, the external sample holder was cooled down with the water of the primary cooling system of the HFR.

The gap between the sample holders were filled with gas, either helium or neon or a mix of the two, in order to adjust the temperature of the experiment.

3. The codes applied for the interpretation

3.1. Neutronics tools

Most benchmark participants used data provided by SERPENT-2, a three-dimensional continuous energy Monte Carlo burnup calculation code mainly for reactor physics applications, developed at the VTT Technical Research Centre of Finland since 2004. The current version 2.2.0 of SERPENT-2 [6] was used for the study. The neutron transport resolution is based on a combination of conventional surface-to-surface ray-tracing and the Woodcock delta-tracking method. Burnup depletion equations are solved using the matrix exponential method CRAM (*Chebyshev Rational Approximation Method*), providing a robust and accurate solution with a very short computation time and is entirely based on built-in calculation routines, without coupling the code to any external solver. A comparison between CRAM, ORIGEN solver and other TTA (*Truncated Taylor Approximation*) methods proved the advantages of the CRAM method in terms of accuracy and running time, thanks to its mathematical approach. Continuous-energy cross-sections read from the library files are reconstructed on a unionized energy grid, used for all reaction modes: the use of a single energy grid results in a significant speed-up in calculation times. Macroscopic cross-sections for each material are pre-generated before the transport simulation: instead of calculating the cross-sections by summing over the constituent nuclides during tracking, the values are read from pre-generated tables, which is another effective strategy useful in order to improve the code overall performance. The pre-generated macroscopic cross-sections are updated at different burnup steps, properly chosen with regards to the irradiation progression. The effect of a neutron spectrum change along irradiation is thus duly taken into account in this way. SERPENT-2 was validated against various criticality benchmarks, experiments, research reactors tests, burnup and full core calculations, duly reported and documented in the manuals of the code.

At KIT a neutronics code and data system, C^4P-TRAIN [7], was employed for generation of self-shielded 560-group cross-sections and for burn-up calculations, using JEFF 3.1.1 data [8]. Neutron transport calculations at several times were performed with a Sn deterministic transport code, DANTSYS [9]. These updates in the neutron transport computations – about 10 along the duration of the experiment – are performed with the goal to take into account variations in the test fuel isotopic composition under irradiation. At every updating time, the microscopic and macroscopic cross-sections in the test fuel region are recalculated, then the neutron flux and radial power profile are recomputed. Two 1D models with white (similar to reflective) radial boundary conditions were employed with DANTSYS: (1) a core model with irradiated pin surrounded by sodium container and other core elements, including driver fuel, and (2) a cell model with irradiated pin surrounded by sodium. As the approximate core model includes part of the reactor core, especially the driver fuel with the cooling water around, the neutron spectrum in this model is quite thermalized due to the moderation by the water: about 95 % of Pu-239 fissions occurs below 0.1 MeV. Whereas the spectrum in the cell model is rather fast, as no moderator is considered: about 55 % of Pu-239 fissions occurs above 0.1 MeV. Therefore, thermal fission product yields (FPYs) for Pu-239 were used for the core model, while fast FPYs were used for the cell one. In addition to C^4P-TRAIN-DANTSYS, also a Monte-Carlo (MC) code, OpenMC [10], was used for cross-checking at KIT at the beginning of

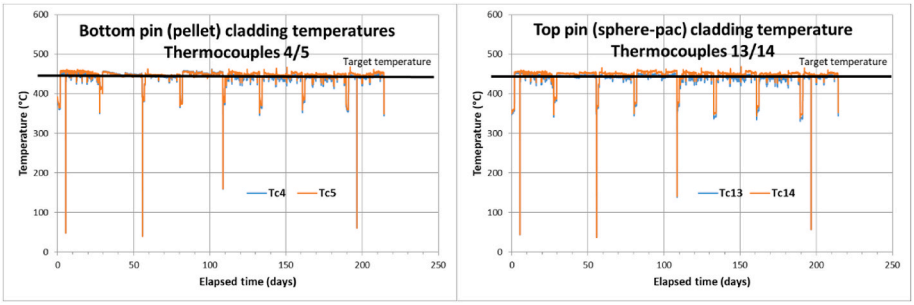

Fig. 1. Monitoring of the middle-height cladding temperatures during the SPHERE experiment in the HFR.

Table 1
SPHERE fuel characteristics.

Pin Nr.	Composition	Isotopic composition	Fuel Density [g cm^{-3}]	^{241}Am contents [g]	^{238}U contents [g]	^{239}Pu contents [g]
#1 Pellets	$U_{0.76}Pu_{0.2}Am_{0.03}$ O_{2-x}	MOX + ^{241}Am	10.393 ≈ 93.8 % TD	0.388	10.192	2.442
#2 Spheres	$U_{0.75}Pu_{0.22}Am_{0.034}$ O_{2-x}	MOX + ^{241}Am	8.33[a]	0.320	7.167	1.869

[a] This overall density takes into account both the density of the sphere and the packing density.

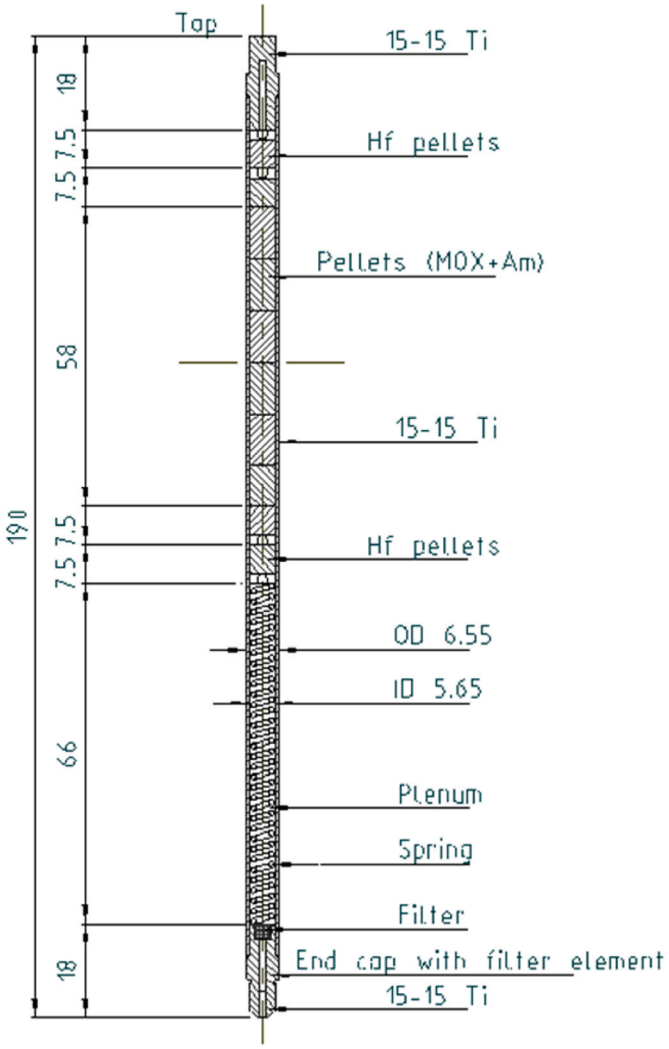

Fig. 2. SPHERE pellet pin.

irradiation.

3.2. Chaining neutronics tools with fuel performance codes

The present work includes neutronics simulations of the experimental device, that are chained with simulations of the irradiation with FPCs. The results obtained with SERPENT-2 were used for simulations with TRANSURANUS and GERMINAL fuel performance codes. Preliminary computations with the FPCs exhibited a clear trend to underestimate both the production and release of fission gases (Xe, Kr) and He. This was due to assumptions about the SPHERE neutron spectrum. Indeed, the assumption of fast spectrum conditions, given the neutron shield surrounding the device, do not reflect accurately the real conditions of the experiment. These may have evolved progressively from those of a hardened neutron flux, targeted by the Hf shield, to more thermalized conditions as irradiation proceeds. Two main consequences are to be considered: firstly, the creation rates of the different isotopes are evolving during the experiment; secondly, the neutron flux and consequently the power created in the fuel are radially heterogeneous, and also varying during the experiment.

It was thus decided to investigate the neutronic conditions of the SPHERE experiment, through dedicated neutronics modelling and simulations of the device. The goal was to derive adequate basic nuclear data to be used as input for the computations with the FPCs: namely, one-energy group averaged cross-sections (fission and capture) and fission yields, being the basic parameters of the point kinetic neutronics modules embedded in FPCs. The radial (and time-dependent) depletion shape of the power in the fuel is also an output of neutronics simulations, and can be provided as an input to the FPCs.

In particular, concerning the TRANSURANUS code, two dedicated source codes were modified and updated according to the outcome of the SERPENT-2 neutronics simulation, for introducing first the tailored cross-sections and then the fission yields related to the Kr, Xe, Nd and Cs isotopes originated form the fission of U-235, Pu-239 and Pu-241.

In case of GERMINAL, the basic nuclear data used by the point kinetic neutronics model are provided in a dedicated input file. New preprocessing tools have been implemented, enabling the possibility of a parameterization of this input file. The tailored data related to the SPHERE experiment, issued from the SERPENT-2 simulation, have been introduced in that way for the GERMINAL computations. Additionally, the possibility to account for a time-dependent radial depletion of the power in fuel was also introduced in the code, as a complementary loading part of the irradiation history.

As the outcome of the neutronics simulation was issued by the SERPENT-2 code in form of a table of numbers (*detector card*), it was necessary to post-process it with a dedicated code written on purpose in Octave language [11], named OVERPROTECT (*OctaVe readEr irRadiation exPeriments cROss-secTions & yiElds CalculaTor*). The code checks all the burnup steps available from the neutronics calculation and asks the user to choose one irradiation time point: then it reads and displays the neutron flux (including fast and thermal components) and the radial profile of the fission power; the code provides also the uranium, plutonium and americium radial distributions. A table of cross-sections is then extracted from the SERPENT's output and organized in tabular format (details are provided in the following Section 4.1 presenting the results from the neutronics simulation). Finally, fission yields for SERPENT are calculated considering the averaged neutron spectrum and the fission cross-sections of the nuclides.

At KIT, the results obtained with C^{4}P-TRAIN-DANTSYS, including the radial power profiles in the pellet and fuel isotopic compositions at different times, for the core (thermal) and cell (fast) models are used for simulations with the fuel performance code FEMAXI [12]. The neutronics results at the beginning of irradiation obtained with different simulation tools at KIT are in general agreement, as shown on Fig. 3 presenting the in-pin power profiles obtained with different options for the core model.

In the C^{4}P-TRAIN models, the test fuel pellet and gap are considered as one region with a radius of 28 mm. This region is subdivided into 10

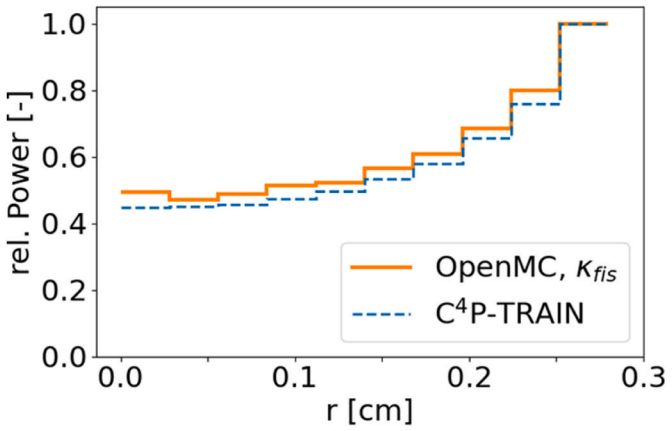

Fig. 3. Radial power profiles in the test pin at the beginning of irradiation computed with C4P-TRAIN-DANTSYS and OpenMC.

radial meshes. The OpenMC and C4P-TRAIN results given in Fig. 3 show the relative power density at the beginning of irradiation in the radial meshes, including the last one with the boundaries of 25 and 28 mm vs the pellet center. The variations of the isotopic composition and radial power profile under irradiation are computed in C4P-TRAIN at several times during irradiation, as already explained in the previous Section 3.1. These variations are further taken into account in the FEMAXI simulations.

3.3. Fuel performance codes and their upgrades

The FPCs applied in the present analysis of SPHERE are: FEMAXI [12], used by KIT; GERMINAL [13], used by CEA; TRANSURANUS version v1m4j22 [14], used by JRC and CVR; the coupled suite TRANSURANUS v1m4j22//SCIANTIX 2.0 [15], developed and used by POLIMI. Advanced versions of the FPCs are herein applied. This is relevant considering the peculiarities of the irradiation experiment, i.e., its capsule set-up and the "hybrid" thermal/fast neutron spectrum conditions. GERMINAL and TRANSURANUS benefit from the nuclear data derived from the specific neutronics modelling of SPHERE, implemented in the respective code burnup modules. The chaining process and the related evolutions introduced for the neutronics modules embedded in the FPCs have been previously described in Section 3.2. For what concerns physics-based models, the application of SCIANTIX 2.0 [15] allows a mechanistic evaluation of the SPHERE fuel swelling and gas release by following the intra- and inter-granular dynamics of Xe, Kr and He. Moreover, advanced laws for Am-bearing fuel properties, based on both experimental and lower-length data and enhancing the physical ground of FPCs, are applied. These include in particular (i) a heat capacity model for MOX fuels in GERMINAL, recently extended to account for the fuel Am content [16], (ii) thermal conductivity and melting temperature models for minor actinide-bearing fuels [17], (iii) models for MOX fuel mechanical properties recently inserted in GERMINAL and TRANSURANUS, including a more mechanistic model for oxide fuel creep.

4. The new interpretation of the SPHERE experiment

4.1. Interpretation with the neutronics tools

4.1.1. Modelling of the SPHERE experiment with the neutronics tools

SERPENT-2 modelling is obtained by simulating only the irradiated pin (as shown on Fig. 4), by imposing as a boundary condition an external flux provided by the SPHERE test experimenters – this flux is calculated with MCNP [18] by simulating the entire core. The simulated pin dimensions are summarized in Table 2, while the neutron flux obtained in the voided pellet position is shown in Fig. 5. The flux in the

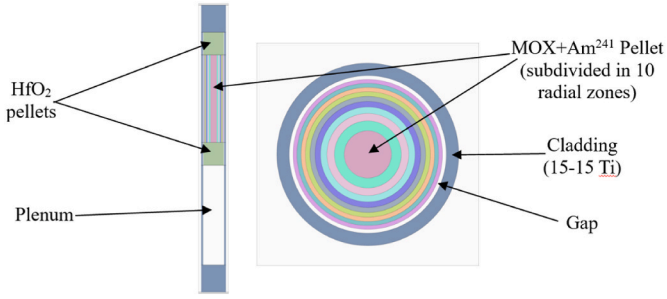

Fig. 4. SERPENT-2 model of the SPHERE irradiated pin.

Table 2
Main characteristics of the SPHERE pellet pin simulated with SERPENT-2.

Pellet diameter (mm)	5.38
Gap size (μm)	13.6
Cladding diameter (mm)	6.55
Cladding material	15-15 Ti
Cladding thickness (mm)	0.45
Fuel weight (g)	13.89
Fuel stack length (mm)	58.92
Free plenum (cm^3)	1.48

voided pellet position is that computed for a fuel rod emptied from any active (i.e. fissile-containing) fuel material. It is issued from the simulation at the scale of the core, performed by the reactor operator. The pin is divided into 10 radial zones in order to track the nuclides distribution evolution during irradiation (although it is not representative of the actual distribution as the neutronics calculation does not take into account thermal gradient re-distribution). The fuel material used for the simulation was a MOX with a 3 % (*weight fraction*) content of Am-241, according to irradiation's report specification (isotopic composition is defined in Table 3); at the bottom and top of the fuel column two HfO_2 (with 2.5 % Y_2O_3) pellets are present and included in the neutronics model. The gap is filled with a gas mixture of He (99 %) and Ne (1 %) at a pressure at room temperature of 0.1 MPa, coherently with the SPHERE experiment specifications.

The adopted cross-sections library is JEFF-3.1.1 [8] and the pin power associated to the irradiation cycles is imposed according to the experimental records provided till 606.19 effective full power days. The power and temperature histories of the simulated pin are shown on Fig. 6 – the plotted temperature corresponding to the maximum clad outer temperature over the pin height, for each irradiation cycle. Fission and capture cross-sections were obtained with SERPENT-2 in the fuel material with 'detectors' using ENDF (*Evaluated Nuclear Data File*) reaction numbers 18 and 102 for total fission and radiative capture, respectively. The simulation is run as a subcritical pin (as the model of the whole core was not available), just defining the neutron flux as the boundary condition (and the power recorded along the experiment). The number of particles simulated in external source mode was 10^7 with an Intel processor i7 (2.67 GHz). The isotopic compositions after irradiation obtained with C4P-TRAIN-DANTSYS for the core model are qualitatively similar to those obtained with SERPENT-2.

4.1.2. Main results from the neutronics simulations

The output of the SERPENT-2 neutronics simulation is the one-group cross-sections table and the neutron spectrum in the pellet at every burnup step defined in the input. These quantities are read by the Octave dedicated program OVERPROTECT in order to issue the one-group cross-sections and fission yields in tabular format, to be further introduced in the FPCs, as previously explained. The code provides a plot of the averaged flux in the pellet, the flux radial profile (for every point defined in the SERPENT-2 input – in this case 10 radial points equally

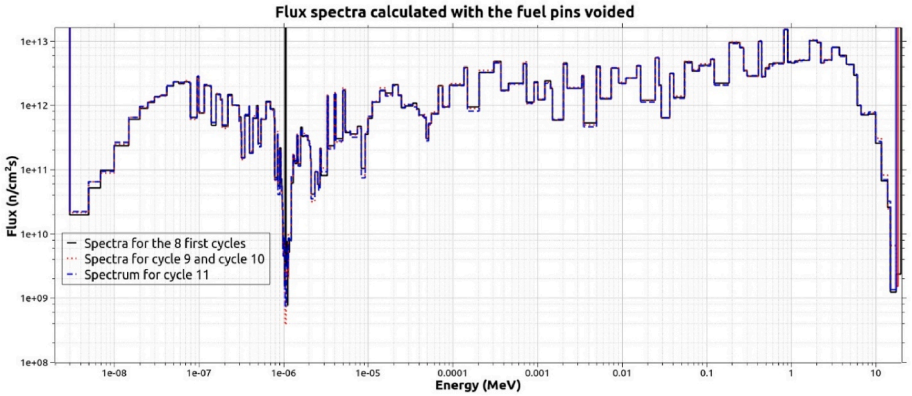

Fig. 5. Neutron spectra calculated in the voided pellet position for the first 8 irradiation cycles (black continuous line), from cycle 9 to 10 (red dotted line) and 11 (blue dashed line). (For interpretation of the references to colour in this figure legend, the reader is referred to the Web version of this article.)

Table 3
Mass composition of the SPHERE pelletized fuel.

Nuclide	wt(%)
U-234	0.0209
U-235	0.1949
U-236	0.0122
U-238	67.5060
Pu-238	0.0031
Pu-239	16.2502
Pu-240	1.6418
Pu-241	0.0222
Pu-242	0.0132
Am-241	2.6040
O-16	11.7313

spaced) and the radial profiles of the thermal and fast flux.

The whole SERPENT-2 calculation was based on a subcritical calculation with an external, imposed source issued from a simulation at the scale of the core, performed by the operator of the experiment. In order to obtain a reasonable value for radially-averaged cross-sections, a proper ratio between a surface and bulk source term had to be investigated and parametrized.

Based on the SERPENT-generated one-group cross-sections, the values considered by the FPCs are averaged quantities between the beginning of irradiation (BOI) and the end of irradiation (EOI), both for fission and capture reactions. The outcome and the structure are reported in Table 5 of Appendix 1, together with the capture/fission values ratio (which was identified as a critical indicator of the reliability of the produced data), in particular concerning Am-241. The neutron capture by Am-241 further leads by chain reaction to the creation of *Cm*-242, which has a very high alpha-decay frequency and is consequently the main contributor to the helium production by a fuel loaded with minor actinides.

Concerning the fission yields, based on the flux in the pellet issued from the neutronics calculation, the yields were calculated with the following (approximate) formula:

$$FPY_Z^A = \frac{\sum_1^i \left[\Phi_i \bullet \sigma_i^{fiss} \bullet FPY_i^{interp}\right]}{\left(\sum_1^i \Phi_i\right) \bullet \sigma_{1-group}^{fiss}} \quad (1)$$

For this purpose, the fission cross-sections of every considered nuclide as a function of energy are stored in an appropriate file to be read by the OVERPROTECT code. The values of the fission yields are interpolated with available data of the JEFF-3.1.1 library. The obtained yields are averaged between beginning and end of irradiation, as it was done for cross-sections. The produced output is reported in Table 6 of Appendix 1.

4.2. Interpretation with the upgraded FPCs

4.2.1. Modelling of the SPHERE experiment with the fuel performance codes

Compared to the first assessment of the SPHERE experiment performed during the PELGRIMM Project [1], the present work relies on refined irradiation and boundary conditions for the fuel performance code simulations. The thermal boundary condition is updated by taking

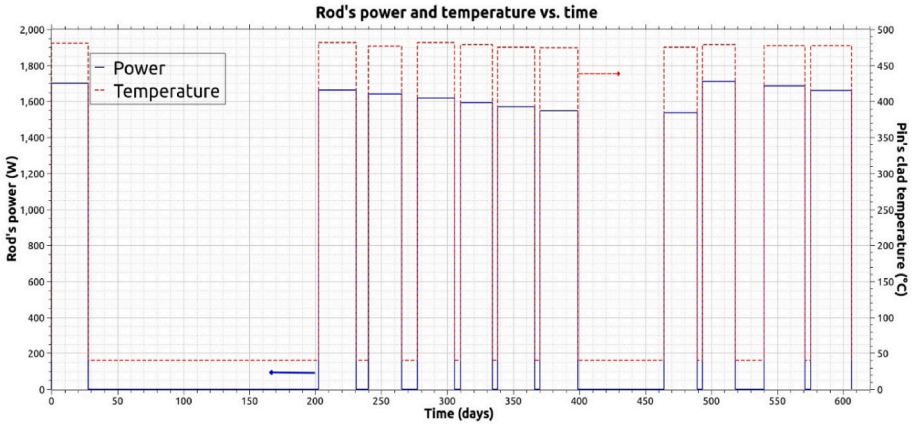

Fig. 6. Power and temperature histories of the SPHERE pellet pin simulated with SERPENT.

into account the temperature monitoring along the experiment, hence the initial assumption of a uniform and time-invariant temperature on the clad outer bound is replaced by a history of an axially varying temperature (Fig. 7 – left showcases the axial clad outer temperature profiles during the first and last SPHERE irradiation cycles). The revision of the linear heat rating history takes into account the measured activities on the fluence monitor sets. As illustrated in Fig. 7 – right, the estimations of the maximum linear heat rating during the first eight cycles of irradiation are significantly increased: from 293 W/cm to 327 W/cm during the first cycle. Details about the clad temperature profiles and the linear power during the SPHERE irradiation cycles are provided in Table 7 of Appendix 2, which also includes the axial distribution of pin linear power (assumed constant along irradiation). The pin geometry and composition are already described in Section 2, while the reference is to Section 4.1 for the nuclear data derived specifically for SPHERE and adopted for the fuel performance code simulations.

For what concerns the neutron spectrum during the SPHERE experiment, as the exact evolution during irradiation of the spectrum conditions inside the experimental assembly could not be easily retrieved (due to uncertainties about the effectiveness and degradation of the Hf shield for thermal neutrons), two bounding assumptions for the FPC computations are adopted. The first option is fast spectrum conditions, corresponding to a flat radial power profile inside the fuel, and the second one is thermal spectrum associated to a time-dependent radial depletion of power in the fuel. Considering these two assumptions for the neutron spectrum, being so far from each other, also means that the uncertainty on the linear heat rating throughout the irradiation may be high. It is unfortunately not possible to provide at this stage an accurate estimation of the uncertainty on the linear heat rating. As previously described, the neutronic simulation of the experiment implements a succession of computational steps, each one combining the evaluation of the neutron spectrum followed by the fuel depletion calculation, using the updated spectrum. There is consequently a cumulation of uncertainties over all the successive computational steps. The estimation of a statistical uncertainty on the linear heat rating throughout the irradiation would thus require multiple independent simulations of the whole experiment. Even if such process remains technically feasible, it would be very costly in computation time, and one should also consider that the number of independent simulations required to obtain a converged estimation of the uncertainty on the linear heat rating can't be defined a priori. This is why such process has not been implemented up to now. For both options of fast or thermal spectrum, a tailored set of basic nuclear data is used, resulting from the neutronics modelling of SPHERE (Section 4.1). The depletion shape which is considered in thermal spectrum corresponds to the default TRANSURANUS model for LWR cases, illustrated in Fig. 8. These profiles are derived from the TRANSURANUS burnup model [19] and reflect the specific evolution of the SPHERE fuel geometry, microstructure and composition during irradiation, i.e., fuel restructuring with the formation of a central hole, as well as a moderate redistribution of Pu towards the hole. The fast/thermal neutron spectrum of the two bounding simulations of SPHERE impacts on irradiation-driven phenomena, e.g., creep of both fuel and cladding.

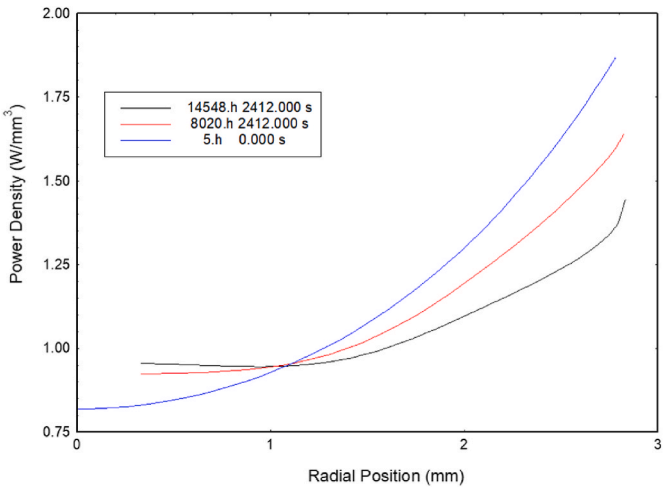

Fig. 8. Radial profiles of power depletion adopted by the fuel performance codes for the "LWR simulation" of SPHERE, in terms of local power density at three representative times during the experiment: 5 h = beginning of irradiation (beginning of cycle 2013-03), 8020.7 h = mid-irradiation (end of cycle 2014-05), 14548.7 h = end of irradiation (end of cycle 2015-03).

As for the modelling setup adopted by the applied codes, different input choices can be selected, appropriate for the "LWR" or "FBR" interpretation of the SPHERE pin performance. As an example, the TRANSURANUS and TRANSURANUS//SCIANTIX simulations rely on different models for the fuel-cladding gap conductance applied under the thermal/fast spectrum assumptions, i.e., the URGAP model [20] or its version adjusted for FR simulations, based on [21]. Another example of dedicated model choice employed concerns the fuel relocation behaviour, impacting the gap width evolution especially at beginning of irradiation. Different relocation parameters are used in FEMAXI for "LWR" and "FBR" simulations of SPHERE, and in parallel, parametric computations have been performed with GERMINAL about the pellet relocation modelling. Concerning the mechanistic inert gas behaviour modelling performed with SCIANTIX, it includes the physics-based consideration of the intra- and inter-granular dynamics of inert gases (Xe, Kr, He), the treatment of the micro-cracking of the fuel grain boundaries, and the percolation of gases from the bubbles on the intact grain boundaries [22]. The helium production rate in the SPHERE fuel is reproduced via a surrogate model which is tailored according to the TRANSURANUS calculations, with regards to the evolution with time along the experiment and the final value of helium produced after irradiation and storage. This modelling choice is supported by the fact that the estimated amount of helium produced from the available neutronics calculations (FISPACT) is lower than the measurement of helium released, leading to more than 100 % of helium fractional release and questioning the reliability of the FISPACT estimation. The main modelling options adopted by the fuel performance codes for the two bounding simulations of the SPHERE irradiation experiment are

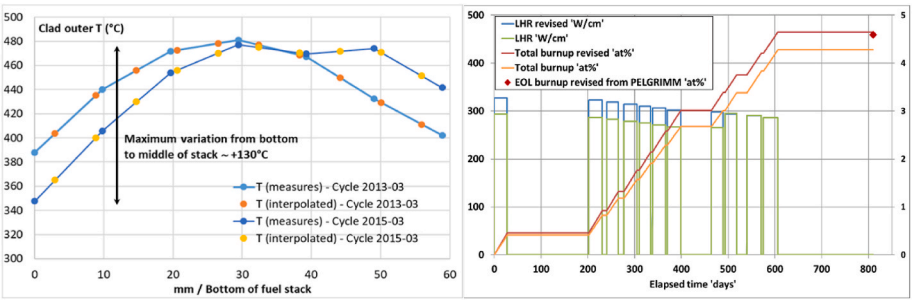

Fig. 7. Revised thermal boundary condition and linear heat rating history.

collected and referenced in Table 8 of Appendix 2.

4.2.2. Main results from the fuel performance code computations

The first FPC results analysed in this paper focus on the production and release of inert gases: namely, fission gases (Xe, Kr) and helium, which is a major concern for fuels bearing minor actinides. The calculation results obtained under both of the assumptions of fast and thermal spectrum are summarized in Table 4, along with the corresponding puncturing examination results on the SPHERE pelletized fuel pin.

The first results analysed here are those for helium production. They are shown on Fig. 9. One can remark that the adoption of a tailored set of basic nuclear data for the SPHERE experiment does not solve all the discrepancies between the computation results. The predictions obtained by GERMINAL and TRANSURANUS do not evolve significantly when moving from fast to thermal spectrum assumption. The SCIANTIX surrogate model for helium production is tailored for retrieving the helium production evolution and final amount according to the TRANSURANUS calculations, thus avoiding the information of more than 100 % release resulting from an estimated helium production via FISPACT which is lower than the released quantity of helium retrieved at puncturing (cf. Table 4). As a consequence for the TRANSURANUS//SCIANTIX suite, there is no difference between the two cases in the computation of helium production. On the contrary, the production computed by FEMAXI//C^{4}P-TRAIN is about 44 % higher in thermal spectrum, compared to that in fast spectrum. The explanation for this discrepancy is the fact that the C^{4}P-TRAIN computations use different sets of (n, alpha) cross-sections and different branching ratios in fast and thermal spectrum. This underlines the need for a complete neutronic characterization of such an experiment like SPHERE. Having determined a tailored set of capture, fission cross-sections and fission yields in the frame of this work only represents a first step in this characterization, to be extended to all basic nuclear data and also completed by considering the depletion of the neutron shield along the experiment. The helium production estimated with FISPACT is more in line with the C^{4}P-TRAIN result in fast spectrum. This tends to confirm the assumption that was retained for the FISPACT computation, regarding the neutron spectrum.

It is then interesting to analyse the predictions obtained for the helium released in the pin free volume, as shown on Fig. 10. There is an overall trend in the results obtained by the codes to underestimate the helium released quantity. This trend is observed with both assumptions of fast or thermal spectrum. The underestimation of the helium released quantity is stronger for the code aligned with FISPACT for the evaluation of the helium production, namely: FEMAXI//C^{4}P-TRAIN in fast spectrum. On the contrary, it is evident from Figs. 9 and 10 that the codes accounting for a helium production greater than the FISPACT estimation are able to reduce the underestimation of the helium released quantity after irradiation and storage, when comparing to the quantity retrieved at puncturing. This indicates that probably more helium than the FISPACT estimation was produced in the SPHERE fuel. Nevertheless, the predictions of helium release by the FPCs remain lower than the measurement, even by using a tailored set of basic nuclear data. Two explanations can be proposed:

- The helium produced and released by the fuel during irradiation, at hot state, is underestimated. This would mean that the creation of the heavy nuclides contributing to the helium production by decay is underestimated during the irradiation.
- Predicting no helium release during storage, prior to puncturing, may not exactly reflect the real behaviour. The reactor temperature at null power is 40 °C, and this temperature looks too low for enabling the helium release by the fuel. But a residual power in the fuel during the storage after irradiation could create a higher temperature in the fuel at that time, enabling – at least partially – the helium diffusion and release.

This firstly confirms the need for refining further the evaluation of the irradiation conditions. But there can be another need for refining the definition of the storage conditions, especially with the goal to evaluate the residual power in the fuel during the storage.

Considering both helium production and release, the assumption of thermal spectrum turns out to be more adequate, especially when considering the helium quantity retrieved in plenum at puncturing. The helium production estimated via FISPACT with the assumption of fast spectrum is much too low to predict correctly the final quantity released in plenum. This explains why the estimation of the helium release rate is greater than 100 % when computed with the evaluation of the helium production by FISPACT.

Regarding the fission gases production – namely, xenon and krypton, the predictions obtained by the FPCs are presented in Fig. 11. Two different trends can be noted: for TRANSURANUS and FEMAXI//C^{4}P-

Table 4
FPCs results for inert gas production and release and puncturing examination results.

FPCs results Option 1 Fast spectrum	Xe + Kr produced (atoms)	Xe + Kr released (atoms)	Xe + Kr release rate (%)	He produced (atoms)	He released (atoms)	He release rate (%)
TRANSURANUS	4.23E+20	2.00E+20	47.2 %	1.77E+20	1.13E+20	63.8 %
TRANSURANUS //SCIANTIX	4.08E+20	2.92E+20	71.6 %	1.20E+20	8.44E+19	70.3 %
GERMINAL	3.65E+20	1.06E+20	29.0 %	1.82E+20	1.28E+20	70.3 %
FEMAXI //C^{4}P-TRAIN	3.67E+20	2.08E+20	56.7 %	1.20E+20	8.25E+19	68.8 %
FPCs results **Option 2** **Thermal spectrum**	Xe + Kr produced (atoms)	Xe + Kr released (atoms)	Xe + Kr release rate (%)	He produced (atoms)	He released (atoms)	He release rate (%)
TRANSURANUS	4.78E+20	3.38E+20	70.6 %	1.80E+20	1.17E+20	65.0 %
TRANSURANUS //SCIANTIX	4.02E+20	3.67E+20	91.3 %	1.19E+20	8.73E+19	73.4 %
GERMINAL	3.64E+20	1.07E+20	29.4 %	1.82E+20	1.29E+20	70.9 %
FEMAXI //C^{4}P-TRAIN	3.92E+20	1.91E+20	48.7 %	1.73E+20	1.23E+20	71.1 %
Experimental data from puncturing N.B. Xe, Kr and He productions issued from computations [a]	Xe + Kr produced (atoms) 4.12E+20	Xe + Kr released (atoms) 3.28E+20	Xe + Kr release rate (%) 79.6 %	He produced (atoms) 1.13E+20	He released (atoms) 1.56E+20	He release rate (%) [b] 138 % [b]

[a] The productions of xenon, krypton and helium used for estimating the release rates with the puncturing results are issued from a FISPACT [23] computation performed by the reactor operator.

[b] The helium release rate exceeding 100 % is a consequence of using of an estimated production issued from computations.

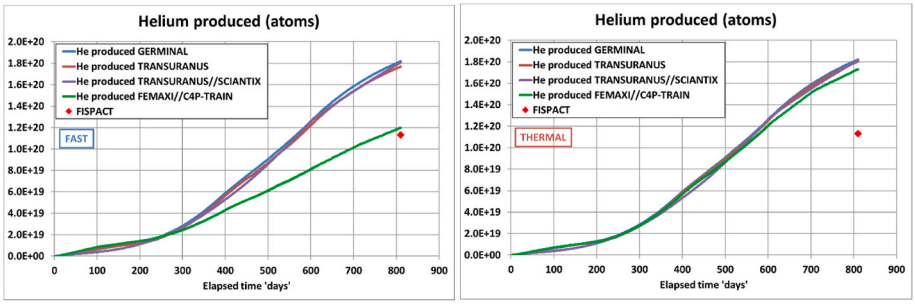

Fig. 9. FPCs results for the helium production.

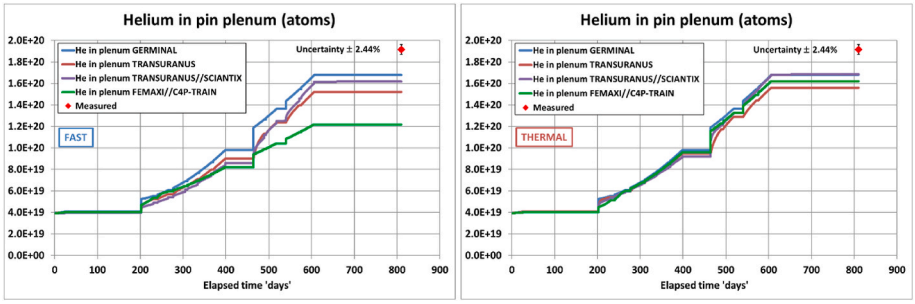

Fig. 10. FPCs results for the helium in the pin free volume.

TRAIN, the production of fission gases is increased when moving from fast to thermal spectrum assumption; whereas it is not really affected by the spectrum conditions, when considering the predictions by TRANSURANUS//SCIANTIX and GERMINAL. This illustrates the fact that not only the cross-sections and the fission yields affect the estimation of the fission gases production, but also the fission energies, that are not the same in fast and thermal spectrum for the TRANSURANUS and FEMAXI//C^{4}P-TRAIN computations. As TRANSURANUS//SCIANTIX and GERMINAL use a single set of values for the fission energies, their predictions for the fission gases production are logically less affected by the neutron spectrum assumption.

This indicates the need to re-evaluate the energy per fission for each nuclide, for the different spectrum conditions of interest. This can be done for example on the basis of the more recent JEFF library together with EPMA data.

The estimation obtained by FISPACT is surrounded by the FPCs results. A higher estimation is obtained by TRANSURANUS in thermal spectrum, indicating that more fissions are needed in these conditions to build up the heat source term, with respect to the given linear heat rating. This is the effect of lower fission energies in thermal spectrum.

The last results related to the inert gases behaviour are the predictions of fission gas release. They are presented in Fig. 12. The predictions of fission gas release are the one showing the highest discrepancies between the codes. Again, two different trends can be noted: for TRANSURANUS and TRANSURANUS//SCIANTIX, the predicted fission gas release is significantly increased when moving from fast to thermal spectrum assumption. This is mostly visible for the TRANSURANUS result. The best agreement with the amount of fission gases retrieved at puncturing is obtained by TRANSURANUS in thermal spectrum. On the other side, the predictions by FEMAXI//C^{4}P-TRAIN and GERMINAL are very slightly changed by the spectrum conditions. There is nearly no change in the results obtained by GERMINAL. These different evolutions are linked to those of the predicted temperatures in the fuel, that are much higher for TRANSURANUS and TRANSURANUS//SCIANTIX with the assumption of thermal spectrum. This will be illustrated and discussed at the end of the section.

For what concerns the fuel restructuring mechanism, Fig. 13 shows the central hole radius at end-of-life predicted by the different codes, along the fuel column, compared with the measurements. One can remark first the scattering of the measures, which could be the consequence of geometrical irregularities along the column, such as pellet eccentricity. The predictions by the codes do not render this effect, as they all adopt an axisymmetrical representation of the geometry. The central hole radii at end-of-life predicted by TRANSURANUS and TRANSURANUS//SCIANTIX are slightly increased in thermal spectrum, despite the radial depletion of power in fuel. The calculated temperatures in the fuel at the beginning-of-life are high enough for enabling an initial fuel restructuring. But the fuel temperatures are evaluated even higher later in irradiation (see Fig. 13 – right): the effect of the gap size decrease along irradiation is not as strong as that of the decrease of the

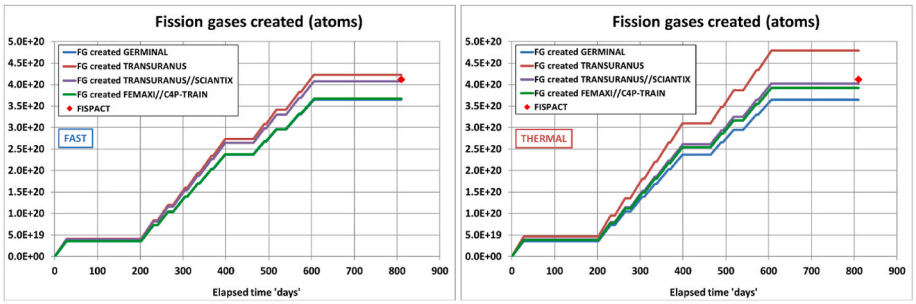

Fig. 11. FPCs results for the fission gases production.

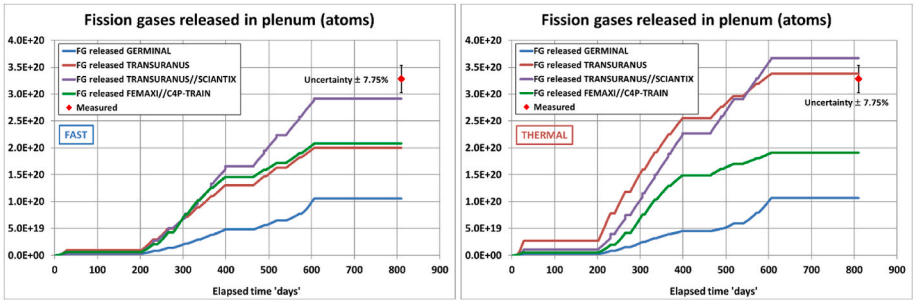

Fig. 12. FPCs results for the release of the fission gases.

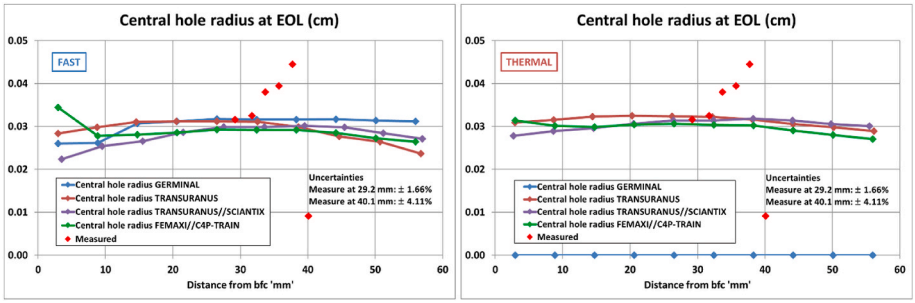

Fig. 13. FPCs results for the central hole radius at end-of-life.

thermal conductivity of the gas mixture in the gap, due to the release of fission gases, the thermal conductivities of which are poor. There is consequently a delayed re-enabling of fuel restructuring, leading to a supplementary increase of the central hole radius. The results obtained by FEMAXI//C^{4}P-TRAIN are not significantly affected by the spectrum conditions. The predicted central hole is a bit wider at the bottom of the fuel column in case of fast spectrum. Regarding the GERMINAL computations, the radial depletion of power in the fuel in thermal spectrum inhibits the fuel restructuring mechanism. The trends observed for FEMAXI//C^{4}P-TRAIN and GERMINAL are also linked with the temperature evolution in the fuel. For these two codes, the peak temperature in fuel is reached at the very beginning of the irradiation, at hot state when the pellet-to-clad gap is still open. Then the maximum temperature along the rest of the irradiation is not as high as at the beginning. For GERMINAL, the threshold for fuel restructuring is exceeded only in the case of fast spectrum, i.e. with a flat radial profile of the power in fuel. The peak temperature at beginning-of-life is thus higher in fast spectrum, enabling the fuel restructuring. In the contrary, the peak temperature at beginning-of-life in thermal spectrum is decreased by the radial depletion of power and consequently not high enough to enable the restructuring mechanism.

Apart from the inhibition of fuel restructuring in thermal spectrum observed for GERMINAL, the predictions by the codes show an overall consistency.

The assessments of the physical mechanisms in the fuel are strongly linked to the temperature evaluation. The evolutions with time of the maximum temperature in the fuel computed by the different codes at the Peak Power Position (namely, at the top of the column) are presented in Fig. 14. The comparison of these results helps explaining the different trends previously seen in the predictions for the gases behaviour and the fuel restructuring.

Concerning first the predictions by TRANSURANUS and TRANSURANUS//SCIANTIX, the models involved for the fuel-cladding gap thermal conductance are different for the computations in fast and thermal spectrum. In fast spectrum, the model is still based on URGAP [20] but takes into account a minimum value for the gap conductance based on data from [21], yielding a better heat removal from the fuel, representative for a faster gap evolution towards closure in fast reactor pins. This represents a first simple approach to take into consideration the effects due to eccentricity [24], that are assumed to be more important in FBR fuels in comparison with LWR fuels. A better, data-driven method based on multi-dimensional analysis with the OFFBEAT code, is under development. As a main consequence, the maximum temperature predicted in the fuel is significantly higher in thermal spectrum (up to 500 °C higher during the cycle #7). This explains why the prediction of fission gas release is strongly increased in thermal spectrum, and also why the fuel restructuring is a bit more enabled in the thermal interpretation of SPHERE, despite the radial depletion of power.

In case of GERMINAL, the same model for the gap conductance is

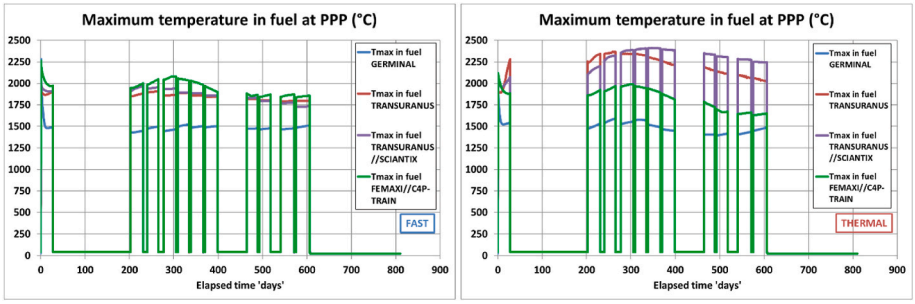

Fig. 14. FPCs results for the maximum temperature in fuel at Peak Power Position.

used for both computations in fast and thermal spectrum. The pellet-to-clad gap closure is predicted to happen very early in the irradiation in case of a fast spectrum, whereas it closes only at the end of irradiation in case of thermal spectrum. These trends are explained by a lower magnitude of pellet relocation in thermal spectrum, as a consequence of a decreased temperature gradient in the pellets, due to the radial depletion of power in the fuel. The associated evolutions of the gap conductance in fast and thermal spectrum are thus coherent: higher gap conductance in fast spectrum with a closed gap, decreasing along irradiation with the release of fission gases; and a lower gap conductance in thermal spectrum, increasing at the end of irradiation with the gap closure. The radial depletion of power in the fuel in thermal spectrum compensates the lower gap conductance. Thus the maximum temperatures reached in the fuel are quite consistent when comparing the computations in fast and thermal spectrum. Anyway, the temperatures calculated by GERMINAL seem to be too low in both cases, with regards to the underestimation of the fission gas release. The highest temperatures over the whole irradiation are predicted at the very beginning of irradiation.

Finally, for the FEMAXI//C^4P-TRAIN computations, the same model for the gap conductance is also used for both cases of fast and thermal spectrum. When comparing the results obtained in the two cases, the gap size and gap conductance evolutions are quite consistent. As a consequence, the slightly lower maximum temperature in fuel predicted in thermal spectrum reflects the effect of the radial depletion of power, decreasing the temperature.

After this review of the main results obtained by the FPCs, one can underline that the predictions of the fuel behaviour in terms of fission gas release and restructuring are fully driven by the temperature calculation, and beyond that by the modelling of the heat transfer between pellet and clad and the correlated evaluation of the pellet-to-clad gap evolution. This observation is completely consistent with the outcomes of previous studies [25,26]. In this work, the consideration of two different options for the neutron spectrum and consequently the possibility of a radial depletion of power in the fuel introduces another cause of discrepancies between the code predictions of the fuel temperature.

5. Conclusion

We present an advanced interpretation of the SPHERE experiment based on the chaining of neutronics simulations with fuel performance code computations. The study also relies on an updated irradiation history and thermal boundary conditions, and investigates different spectrum conditions. The comparison of the computation results with experimental data focuses on the inert gas production and release – helium and fission gases, and on the fuel restructuring.

The main outcomes and perspectives are the following:

- With regards to the helium production and release, it turns out that the spectrum conditions for the SPHERE experiment shall have been closer to those in a thermal reactor, despite the hafnium neutron shield intending to harden the flux in the device. Considering the remaining discrepancies between computation results and the experimental data, the need for a complete neutronic characterization of the experiment is confirmed, with the goal to provide to the FPCs a complete set of basic nuclear data, evolving with time, in linked with the progressive depletion of the neutron shield along the experiment. Such investigations about the performance of neutron shields have been realized [27] in link with the implementation of the AFC-2C and AFC-2D transmutation experiments with oxide fuel in the Advanced Test Reactor [28]. These investigations are absolutely necessary in case of an experiment performed in a Material Testing Reactor, with a device intending to create peculiar spectrum conditions that differ from the standard conditions of the reactor where the experiment is operated. Concerning the SPHERE experiment, the evolution of the neutronic conditions with time shall be investigated in link with the successive positions of the device in the core, and during all the different cycles of the irradiation. In this work, a first progression towards such neutronic characterization has been obtained, and is to be pursued.
- The systematic underestimation by the codes of the helium quantity retrieved in plenum also suggests to investigate the fuel conditions during the storage. The possibility that a residual power in the fuel may have enabled, at least partially, the release of the helium created by alpha-decays during the storage, is to be considered.
- These investigations about the overall conditions of the experiment from the beginning of the irradiation to the end of the storage are the prerequisite for assessing the capabilities of the FPCs to simulate the SPHERE fuel behaviour in the HFR.
- As a further perspective for the simulation tools, an extended (online) coupling between neutronics tools and FPCs could be envisaged. The feedback of the geometrical and thermal evolutions of the fuel on the neutronic conditions, besides e.g., the impact of the cooling environment, could thus be taken into account.
- Another perspective for the experimental work could be to perform advanced post-irradiation examinations of the SPHERE fuel, with one particular goal to evaluate more accurately the americium transmutation performance.

CRediT authorship contribution statement

Marc Lainet: Writing – review & editing, Writing – original draft, Visualization, Validation, Supervision, Software, Resources, Methodology, Investigation, Data curation, Conceptualization. **Lelio Luzzi:** Writing – review & editing, Validation, Supervision, Project administration, Methodology, Funding acquisition, Conceptualization. **Alessio Magni:** Writing – review & editing, Writing – original draft, Visualization, Validation, Software, Resources, Methodology, Investigation, Conceptualization. **Davide Pizzocri:** Writing – review & editing, Validation, Software, Resources, Methodology, Investigation, Conceptualization. **Martina Di Gennaro:** Validation, Software, Resources, Investigation. **Paul Van Uffelen:** Writing – review & editing, Validation, Software, Resources, Methodology, Investigation, Conceptualization. **Arndt Schubert:** Writing – review & editing, Validation, Software, Resources, Methodology, Investigation, Conceptualization. **Elio D'Agata:** Writing – review & editing, Writing – original draft, Validation, Resources, Methodology, Investigation, Conceptualization. **Vincenzo Romanello:** Writing – review & editing, Writing – original draft, Visualization, Validation, Software, Resources, Methodology, Investigation, Conceptualization. **Andrei Rineiski:** Writing – review & editing, Writing – original draft, Visualization, Validation, Software, Resources, Methodology, Investigation, Conceptualization. **Karl Sturm:** Writing – review & editing, Visualization, Validation, Software, Resources, Methodology, Investigation, Conceptualization. **Sander Van Til:** Writing – review & editing, Validation, Methodology, Investigation, Data curation, Conceptualization. **Florence Charpin:** Writing – review & editing, Validation, Software, Methodology, Investigation, Data curation, Conceptualization. **Alexander Fedorov:** Writing – review & editing, Validation, Methodology, Investigation, Data curation, Conceptualization.

Declaration of competing interest

The authors declare that they have no known competing financial interests or personal relationships that could have appeared to influence the work reported in this paper.

Acknowledgements

This work has received funding from the Euratom research and training programme 2019–2020 under grant agreement No 945077 (PATRICIA Project).

Appendix 1. Results from the neutronics simulations used on input by the fuel performance codes

Table 5
Fission and capture cross-sections at the BOI and EOI, their average and ratio computed with SERPENT-2

Nuclide	FissXS_BOI	CaptXS_BOI	FissXS_EOI	CaptXS_EOI	*FissXS_aver*	*CaptXS_aver*	*Capt/Fiss*
U-234	0.743972	9.12681	0.735301	10.5624	*0.740*	*9.845*	*13.3*
U-235	12.0319	3.09394	12.706	3.16224	*12.369*	*3.128*	*0.3*
U-236	0.303893	1.9287	0.302516	2.0638	*0.303*	*1.996*	*6.6*
U-238	0.0786835	0.380611	0.0764123	0.404253	*0.078*	*0.392*	*5.1*
U-239	0.730064	1.89387	0.756083	1.90559	*0.743*	*1.900*	*2.6*
Np-237	0.854008	13.7039	0.844389	14.1884	*0.849*	*13.946*	*16.4*
Np-238	37.3667	3.75668	40.1807	4.03901	*38.774*	*3.898*	*0.1*
Np-239	1.00561	7.14152	0.996624	7.31763	*1.001*	*7.230*	*7.2*
Pu-238	2.15938	7.173	2.10413	7.91169	*2.132*	*7.542*	*3.5*
Pu-239	19.9388	8.98851	21.9027	10.0494	*20.921*	*9.519*	*0.5*
Pu-240	0.888979	11.1436	0.882237	11.3837	*0.886*	*11.264*	*12.7*
Pu-241	23.085	7.48475	25.179	8.257	*24.132*	*7.871*	*0.3*
Pu-242	0.793909	6.75086	0.786217	7.8179	*0.790*	*7.284*	*9.2*
Pu-243	9.28288	4.34004	9.49124	4.44079	*9.387*	*4.390*	*0.5*
Am-241	0.906101	24.5003	0.909857	26.4179	*0.908*	*25.459*	***28.0***
Am-242	47.1781	5.82107	50.5868	6.09906	*48.882*	*5.960*	*0.1*
Am-242 m	133.536	25.3404	145.495	27.651	*139.516*	*26.496*	*0.2*
Am-243	0.565361	17.4037	0.559781	17.3398	*0.563*	*17.372*	*30.9*
Cm-242	1.60527	5.53658	1.5546	4.89938	*1.580*	*5.218*	*3.3*
Cm-243	22.878	3.46352	24.1851	3.67082	*23.532*	*3.567*	*0.2*
Cm-244	1.20628	2.70474	1.21012	3.38071	*1.208*	*3.043*	*2.5*
Cm-245	33.1655	5.04772	35.5422	5.41745	*34.354*	*5.233*	*0.2*

Appendix 2. Details about the modelling of the SPHERE experiment with the fuel performance codes

Table 6
Fractional fission yields calculated with the OVERPROTECT tool, further used on input by the TRANSURANUS and GERMINAL FPCs

	U-234	U-235	U-236	U-238	Np-237	Np-238	Pu-238	Pu-239	Pu-240	Pu-241	Pu-242	Am-241	Am-242 m	Am-243	*Cm*-243	*Cm*-244	*Cm*-245
Kr-83	0.007765	0.005827	0.005952	0.003436	0.004877	0.003378	0.003002	0.002987	0.002308	0.002037	0.001806	0.002700	0.002168	0.001244	0.001213	0.001366	0.001317
Kr-84	0.012600	0.010622	0.010234	0.006843	0.007964	0.006382	0.004618	0.004951	0.004130	0.003747	0.003604	0.004090	0.002721	0.002005	0.001899	0.002061	0.002045
Kr-85	0.003874	0.002892	0.002954	0.001864	0.002042	0.001781	0.001499	0.001365	0.000957	0.000918	0.000682	0.001272	0.000834	0.000624	0.000651	0.000652	0.000783
Kr-86	0.025528	0.020242	0.019456	0.012182	0.013385	0.010912	0.009745	0.007982	0.006532	0.006287	0.005457	0.007835	0.005553	0.004383	0.004105	0.004270	0.006326
Nd-143	0.051152	0.057218	0.051152	0.046058	0.047128	0.043626	0.044854	0.044103	0.045236	0.044476	0.045815	0.038594	0.043215	0.041439	0.041037	0.043538	0.043884
Nd-144	0.042862	0.052570	0.047204	0.045701	0.041227	0.037457	0.039041	0.036643	0.039798	0.041424	0.042890	0.034095	0.041939	0.039288	0.034558	0.040229	0.040825
Nd-145	0.035247	0.038548	0.042478	0.038023	0.032161	0.038203	0.033577	0.030361	0.031377	0.031822	0.033914	0.035532	0.038174	0.035904	0.033257	0.035216	0.032331
Nd-146	0.027342	0.029460	0.034917	0.034878	0.028111	0.033385	0.027026	0.025074	0.025769	0.026833	0.029195	0.029402	0.030847	0.030054	0.026230	0.031202	0.027544
Nd-148	0.014112	0.016662	0.019527	0.022130	0.017418	0.018091	0.016459	0.016722	0.017979	0.019012	0.020242	0.019305	0.021915	0.020610	0.018241	0.023440	0.025960
Nd-150	0.006160	0.006706	0.010079	0.012812	0.009859	0.009356	0.008460	0.009859	0.010654	0.011686	0.013169	0.012578	0.002799	0.012753	0.006248	0.014600	0.006284
Cs-133	0.073178	0.065829	0.066532	0.066255	0.066912	0.067955	0.069819	0.070062	0.069835	0.066314	0.068301	0.057957	0.053601	0.055086	0.053959	0.050748	0.054004
Cs-134	0.000004	0.000003	0.000000	0.000000	0.000003	0.000000	0.000052	0.000008	0.000002	0.000000	0.000000	0.000025	0.000003	0.000001	0.000079	0.000027	0.000004
Cs-135	0.077665	0.064890	0.061551	0.063473	0.076160	0.075183	0.077772	0.074403	0.075614	0.070985	0.068896	0.071277	0.070127	0.070290	0.065754	0.064018	0.062061
Cs-137	0.061652	0.060584	0.057881	0.059857	0.062663	0.069359	0.064344	0.065020	0.065276	0.063107	0.061486	0.065968	0.061473	0.064278	0.072522	0.065892	0.066710
Cs-139	0.061154	0.062797	0.063322	0.057646	0.055667	0.053955	0.049858	0.055245	0.056628	0.059785	0.059020	0.062030	0.055669	0.055384	0.052407	0.051877	0.062889
Xe-131	0.029039	0.031220	0.029857	0.033477	0.037342	0.030720	0.035474	0.038561	0.035716	0.031034	0.030971	0.039498	0.034944	0.035233	0.032831	0.029980	0.031004
Xe-132	0.053211	0.044812	0.040527	0.047513	0.046880	0.047997	0.054276	0.052390	0.046522	0.045491	0.044860	0.047371	0.043349	0.044785	0.045120	0.039807	0.043274
Xe-134	0.080692	0.077374	0.077107	0.067853	0.073511	0.065622	0.078438	0.071087	0.071879	0.075905	0.073452	0.062340	0.063203	0.063846	0.064466	0.059853	0.058898
Xe-136	0.070440	0.064627	0.068313	0.072184	0.070552	0.080917	0.067685	0.069881	0.067076	0.070381	0.072106	0.066236	0.067165	0.071106	0.066258	0.062155	0.051095
He-4	0.002309	0.001699	0.001899	0.001428	0.002060	0.001860	0.002420	0.002191	0.002781	0.001860	0.002370	0.002370	0.002100	0.001820	0.002580	0.002420	0.002280

Table 7
Details about the revised thermal boundary condition (axial profiles of cladding outer temperature) and linear heat rating history along the cycles of the SPHERE irradiation.

	Fuel axial discretization: slice number (mm/bottom of fuel stack)										
	1 (2.95)	2 (8.84)	3 (14.73)	4 (20.62)	5 (26.51)	6 (32.40)	7 (38.29)	8 (44.19)	9 (50.08)	10 (55.97)	
Cycle	Cladding outer temperature (°C) at the corresponding axial positions										Max Linear Heat Rate[a] (W/cm)
2013–03	403.8	435.1	456.0	472.6	478.3	476.9	468.5	449.7	429.3	411.1	327.05
2014–02	400.3	430.5	451.3	468.4	477.1	477.3	469.0	461.2	446.0	393.3	322.43
2014–03	394.4	424.6	447.3	466.1	472.8	471.7	462.8	459.4	451.8	417.3	318.15
2014–04	399.0	429.7	451.0	468.7	477.6	477.2	467.7	459.6	445.3	398.6	314.21
2014–05	383.0	414.2	440.6	463.3	472.5	474.0	467.8	464.4	457.5	430.1	309.93
2014–06	394.1	422.8	446.8	466.9	472.8	471.2	462.2	459.6	453.1	420.8	306.16
2014–07	391.6	420.9	445.7	466.6	472.5	470.8	461.3	460.3	455.9	425.9	301.71
2014–08	394.6	422.8	446.9	467.1	472.4	470.3	460.6	459.4	454.8	424.4	297.26
2015–01	380.6	414.3	442.9	467.2	474.9	474.1	464.8	464.9	461.0	426.8	294.01
2015–02	379.9	414.4	442.5	466.3	474.2	473.8	464.9	466.0	463.4	432.3	289.9
2015–03	365.1	400.1	429.9	456.2	470.2	474.9	470.4	471.9	470.9	451.3	285.62
LHR axial peak factors	0.94	0.95	0.95	0.96	0.97	0.97	0.98	0.99	0.99	1	

[a] The linear heat rate provided in this table corresponds to the maximum value experienced by the fuel during the SPHERE irradiation (i.e., at axial slice 10 where peak factor is 1).

Table 8
Details about the main modelling options adopted by the fuel performance codes for the simulations of the SPHERE irradiation experiment.

Option 1 Fast spectrum ("FBR simulation")	TRANSURANUS	TRANSURANUS //SCIANTIX	GERMINAL[a]	FEMAXI[b]
Gap conductance	URGAP model modified for FBR conditions [21]	URGAP model modified for FBR conditions [21]	Arnaud-Roche model	Ross & Stoute model
Fuel relocation	Model calibrated on liquid-metal FBR	Model calibrated on liquid-metal FBR	Empirical correlation to the temperature gradient	SIEX code correlation [29]
Fuel densification	Pore migration model for FBR conditions	Pore migration model for FBR conditions	Empirical correlation to the temperature	Schlemmer & Ichikawa model
Fuel thermal conductivity	[17]	[17]	[17]	[30]
Fission gas production	Fission yields for Xe and Kr from SPHERE neutronic modelling (Section 4.1.2) **Flat radial power profile**	Fission yields for Xe and Kr, from [31] **Flat radial power profile**	Point kinetic neutronics model **Flat radial power profile**	Neutronics by C^4P-TRAIN in **fast spectrum**
Helium production	From TUBRNP (TRANSURANUS burnup module), including fission yields for He from SPHERE neutronic modelling (Section 4.1.2)	Surrogate model tailored for SPHERE	Point kinetic neutronics model	Neutronics by C^4P-TRAIN
Helium release	Based on He diffusion according to [32]	Treated by SCIANTIX physics-based module	Temperature threshold for helium release	Power threshold for helium release
Inert gas behaviour	Semi-empirical TRANSURANUS model for FBR conditions	Treated by SCIANTIX physics-based module	Fission gas release model	Mechanistic fission gas release model
Option 2 Thermal spectrum ("LWR simulation")	TRANSURANUS	TRANSURANUS //SCIANTIX	GERMINAL[a]	FEMAXI[b]
Gap conductance	URGAP model [20]	URGAP model [20]	Same as option 1	Same as option 1
Fuel relocation	Modified FRAPCON-3 model	Modified FRAPCON-3 model	Same as option 1	Same as option 1
Fuel densification	Empirical model for LWR conditions	Empirical model for LWR conditions	Same as option 1	Same as option 1
Fuel thermal conductivity	[17]	[17]	Same as option 1	Same as option 1
Fission gas production	Fission yields for Xe and Kr from SPHERE neutronic modelling (Section 4.1.2) **Radial depletion of power in fuel**	Fission yields for Xe and Kr, from [31] **Radial depletion of power in fuel**	Point kinetic neutronics model **Radial depletion of power in fuel**	Neutronics by C^4P-TRAIN in **thermal spectrum**
Helium production	From TUBRNP (TRANSURANUS burnup module), including fission yields for He from SPHERE neutronic modelling (Section 4.1.2)	Surrogate model tailored for SPHERE	Point kinetic neutronics model	Neutronics by C^4P-TRAIN
Helium release	Based on He diffusion according to [32]	Treated by SCIANTIX physics-based module	Same as option 1	Same as option 1
Inert gas behaviour	Mechanistic TRANSURANUS model for LWR conditions	Treated by SCIANTIX physics-based module	Same as option 1	Same as option 1
Cladding properties/ behaviour	TRANSURANUS models for 15-15Ti stainless steel	TRANSURANUS models for 15-15Ti stainless steel	AIM1	Stainless steel 15-15Ti

[a] The models implemented in GERMINAL and used for this study are mainly described in [13], except the law for the fuel thermal conductivity [17].

[b] The models implemented in FEMAXI and used for this study are mainly described in [33]. except the law for the fuel thermal conductivity [30]. The neutronics analysis is performed by C^{4}P-TRAIN [7] prior to the FEMAXI computation, providing the fission gas and helium productions on input.

References

[1] E. D'Agata, et al., SPHERE: irradiation of sphere-pac fuel of $UPuO_{2-x}$ containing 3% Americium, Nucl. Eng. Des. 275 (2014) 300–311, https://doi.org/10.1016/j.nucengdes.2014.05.021.

[2] A. Gallais-During, et al., Outcomes of the PELGRIMM project on Am-bearing fuel in pelletized and spherepac forms, J. Nucl. Mater. 512 (2018) 214–226, https://doi.org/10.1016/j.jnucmat.2018.10.016.

[3] European Commission, FAIRFUELS Euratom Project, 2015. https://cordis.europa.eu/project/id/232624.

[4] European Commission, PELGRIMM Euratom Project, 2017. https://cordis.europa.eu/project/id/295664.

[5] European Union's Horizon 2020 Research and Innovation programme, Patricia - partitioning and transmuter research Initiative in a Collaborative Innovation action. https://patricia-h2020.eu/, 2020.

[6] J. Leppänen, Serpent – a continuous-energy Monte Carlo reactor physics burnup calculation code, User's Manual (2015). http://montecarlo.vtt.fi/download/Serpent_manual.pdf.

[7] A. Rineiski, V. Sinitsa, C4P-TRAIN neutronics tool for supporting Safety studies of Innovative fast reactors. PHYTRA4 – the Fourth International Conference on Physics and Technology of Reactors and Applications, on CD-ROM, Marrakech, Morocco, 2018.

[8] A. Santamarina, et al., The JEFF-3.1.1 nuclear data library, ISBN 978-92-64-99074-6, NEA No. 6807, https://www.oecd-nea.org/jcms/pl_14470/the-jeff-3-1-1-nuclear-data-library?details=true, 2009.

[9] R.E. Alcouffe, et al., "DANTSYS: A Diffusion Accelerated Neutral Particle Transport Code System", LA-12969- M, Los-Alamos, 1995.

[10] P.K. Romano, et al., OpenMC: a state-of-the-art Monte Carlo code for research and development, Ann. Nucl. Energy 82 (2015) 90–97, https://doi.org/10.1016/j.anucene.2014.07.048.

[11] J.W. Eaton, et al., GNU Octave – A High-Level Interactive Language for Numerical Computations, 2016. Edition 4 for Octave version 4.2.1.

[12] T. Okawa, et al., Fuel behavior analysis code FEMAXI-FBR development and validation for core disruptive accident, Prog. Nucl. Energy 82 (2015) 80–85, https://doi.org/10.1016/j.pnucene.2014.11.002.

[13] M. Lainet, et al., GERMINAL, a fuel performance code of the PLEIADES platform to simulate the in-pile behaviour of mixed oxide fuel pins for sodium-cooled fast reactors, J. Nucl. Mater. 516 (2019) 30–53, https://doi.org/10.1016/j.jnucmat.2018.12.030.

[14] A. Magni, et al., The TRANSURANUS fuel performance code, in: Nuclear Power Plant Design and Analysis Codes - Development, Validation and Application, 2021-1, pp. 161–205, https://doi.org/10.1016/B978-0-12-818190-4.00008-5.

[15] D. Pizzocri, et al., SCIANTIX open-source code for fission gas behaviour: objectives and foreseen developments, in: IAEA Technical Meeting on the Development and Application of Open-Source Modelling and Simulation Tools for Nuclear Reactors, 2022. Milano, Italy.

[16] B. Labonne, et al., Development of an interatomic potential for mixed uranium-americium oxides and application to the determination of the structural and thermodynamic properties of $(U,Am)O_2$ with americium contents below 50, J. Nucl. Mater. 579 (2023), https://doi.org/10.1016/j.jnucmat.2023.154390.

[17] A. Magni, et al., Modelling of thermal conductivity and melting behaviour of minor actinide-MOX fuels and assessment against experimental and molecular dynamics data, J. Nucl. Mater. 557 (2021-2), https://doi.org/10.1016/j.jnucmat.2021.153312.

[18] J.A. Kulesza, et al., MCNP code version 6.3.0 - Theory & user manual, LA-UR-22-30006, Rev 1 (2022). https://mcnp.lanl.gov/pdf_files/TechReport_2022_LANL_LA-UR-22-30006Rev.1_KuleszaAdamsEtAl.pdf.

[19] P. Botazzoli, et al., Extension and validation of the TRANSURANUS burn-up model for helium production in high burn-up LWR fuels, J. Nucl. Mater. 419 (2011) 329–338, https://doi.org/10.1016/j.jnucmat.2011.05.040.

[20] K. Lassmann, F. Hohlefeld, The revised URGAP model to describe the gap conductance between fuel and cladding, Nucl. Eng. Des. 103 (1987) 215–221, https://doi.org/10.1016/0029-5493(87)90275-5.

[21] M. Charles, M. Bruet, Gap conductance in a fuel rod: modelling of the FURET and CONTACT results, in: IAEA, International Working Group on Water Reactor Fuel Performance and Technology, IWGFPT/19, "Water Reactor Fuel Element Performance Computer Modelling", Meeting Proceedings, 1984. https://inis.iaea.org/collection/NCLCollectionStore/_Public/16/057/16057359.pdf.

[22] G. Zullo, et al., The SCIANTIX code for fission gas behaviour: Status, upgrades, separate-effect validation, and future developments, J. Nucl. Mater. 587 (2023), https://doi.org/10.1016/j.jnucmat.2023.154744.

[23] J.-Ch Sublet, et al., FISPACT-II: an advanced simulation system for Activation, transmutation and material modelling, Nucl. Data Sheets 139 (2017) pp77–137, https://doi.org/10.1016/j.nds.2017.01.002.

[24] A. Scolaro, et al., Investigation on the effect of eccentricity for fuel disc irradiation tests, Nucl. Eng. Technol. 53 (2021) 1602–1611, https://doi.org/10.1016/j.net.2020.11.003.

[25] N. Chauvin, et al., Benchmark Study on Innovative Fuels for Fast Reactors with Fuel Performance Codes, 2023. NEA/NSC/R(2022)5, https://www.oecd-nea.org/jcms/pl_79983/benchmark-study-on-innovative-fuels-for-fast-reactors-with-fuel-performance-codes.

[26] J. Lavarenne, et al., Burn-up dependent modeling of fuel-to-clad gap conductance and temperature predictions for mixed-oxide fuel in the ESFR-SMART core, J. Nucl. Eng. Radiat. Sci. 8 (2022), https://doi.org/10.1115/1.4050479.

[27] G.S. Chang, Cadmium depletion impacts on hardening neutron spectrum for advanced fuel testing in ATR, in: International Conference on Mathematics and Computational Methods Applied to Nuclear Science and Engineering, Rio de Janeiro, Brazil, 2011. ISBN 978-85-63688-00-2, https://inis.iaea.org/collection/NCLCollectionStore/_Public/48/031/48031790.pdf?r=1.

[28] H.J. MacLean, S.L. Hayes, Irradiation of Metallic and Oxide Fuels for Actinide Transmutation in the ATR, 2007. Global 2007, Boise, Idaho, USA, https://citeseerx.ist.psu.edu/document?repid=rep1&type=pdf&doi=31c494e9cd15a8b950f4fd4d98a74ab962a3c7be.

[29] D.S. Dutt, R.B. Baker, Siex – a correlated code for the prediction of Liquid metal fast breeder reactor (LMFBR) fuel thermal performance, HEDL-TME 74-55 UC-79b, https://doi.org/10.2172/4181413, 1975.

[30] Y. Philipponneau, Thermal conductivity of $(U,Pu)O_{2-x}$ mixed oxide fuel, J. Nucl. Mater. 188 (1992) pp194–197, https://doi.org/10.1016/0022-3115(92)90470-6.

[31] T. Motta, D.R. Olander, Light Water Reactor Materials, Volume I: Fundamentals, American Nuclear Society Scientific Publications, 2017.

[32] É. Fédérici, et al., Helium production and behaviour in nuclear fuels during irradiation in LWR, in: Proceedings of the International LWR Fuel Performance Meeting, San Francisco, USA, 30 Sep. – 3 Oct. 2007, 2007, pp. 664–673 (paper 1057).

[33] M. Suzuki, H. Saitou, Light water reactor fuel analysis code FEMAXI-6 (Ver.1) – detailed structure and User's manual, JAEA/Data/Code 2005-003 (2005). https://jopss.jaea.go.jp/pdfdata/JAEA-Data-Code-2005-003.pdf.